ACS OMEGA

http://pubs.acs.org/journal/acsodf

Article

Development of Distillation Sensors for Spirit Beverages Production Monitoring Based on Impedance Spectroscopy Measurement and Partial Least-Squares Regression

Liming Zeng,* Arnaud Pernet, Marilyn Cléroux, Benoît Bach, Lucas Froidevaux, and Ioana Preda

Cite This: *ACS Omega* 2023, 8, 15323−15333

Read Online

ACCESS | Metrics & More | Article Recommendations

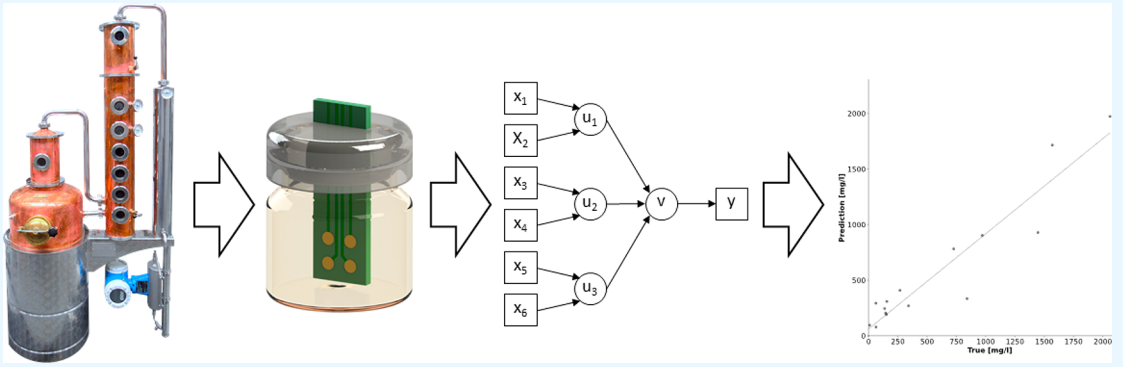

ABSTRACT: During spirit beverages production, the distillate is divided into three parts: the head, the heart, and the tail. Acetaldehyde and ethanol are two key markers which allow the correct separation of distillate. Being toxic, the elimination of the head part, which contains a high concentration of acetaldehyde, is crucial to guarantee the consumer's health and security. Plus, the tail should be separated from the heart based on ethanol concentration. Nowadays, online or in-line sensors for acetaldehyde monitoring during distillation do not exist, and the online sensors for alcohol monitoring, based on density measurement, remain expensive for producers. In this work, we demonstrate the development of distillation monitoring sensors based on electrical impedance spectroscopy (EIS) measurements, combined with PLS-R (partial least-squares regression) modeling. Four types of sensors are proposed and tested with wine-based distillates. Using PLS-R, the best correlations were found for one electrode, named "SpotsSym". With an R^2 up to 89.9% for acetaldehyde concentration prediction and an R^2 up to 86.8% for ethanol, the obtained results indicate the promising potential of the proposed approach. To our knowledge, this is the first report of sensors capable of simultaneously measuring ethanol and acetaldehyde concentrations. Furthermore, these sensors offer the advantages of being low cost and nondestructive. Based on these results, the development of an in-line distillation monitoring system is possible in the near future, providing a promising tool for spirit beverages producers.

INTRODUCTION

Nowadays, portable, low-cost sensors used for the detection of specific chemicals in liquid media are finding an ever-growing demand in various application fields, from the food industry to medical diagnostics and environmental monitoring of contaminants and pollutants.[1] For all of these applications, classical analysis techniques exist, but they are usually expensive and require highly trained personnel, on top of prolonged processing times.[2] Recently, numerous research studies have focused on finding alternatives that are low cost, fast, and, ideally, nondestructive, especially for food product monitoring systems. Among these, electrical impedance spectroscopy (EIS), which applies a small alternating current signal to a sample to generate subsequent electrical responses, is a rather popular alternative for avoiding complex and time-consuming experimental or laboratory procedures, as it quickly measures the electrical impedance of a specimen across a given range of frequencies. While being nondestructive, it provides impedance spectra that can then be used to characterize the physicochemical properties of the investigated system.[3]

The field of spirit beverage production is of no exception, with the development of sensors for the evaluation of ethanol

Received: January 24, 2023
Accepted: April 5, 2023
Published: April 17, 2023

and acetaldehyde concentrations during distillation being particularly important for monitoring processes.

Spirits are alcoholic beverages produced from a variety of agricultural raw materials, such as fruits (grape, apple, apricot, cherry), cereals (barley, wheat, corn), and other plants (sugar cane, gentiane, gin botanicals). The production process for most spirits typically involves several stages, including raw material extraction, yeast fermentation, distillation of the fermented wash, aging of the distillate, and final dilution with water.

The role of distillation is to capture the essence of the raw material while eliminating hazardous substances for human consumption. The distillate is divided into three parts according to its components and its quality: the head, the heart, and the tail. The head is the first part of the distilled liquid to be produced and mainly contains substances that would give an unpleasant sour taste, as well as acetaldehyde, which is toxic and therefore needs to be eliminated. In alcoholic beverages, acetaldehyde may be formed by yeast, acetic acid bacteria, and coupled auto-oxidation of ethanol and phenolic compounds.[4] At high levels, this compound is regarded as possibly carcinogenic to humans (IARC Group 2B).[5] During distillation, the concentration of acetaldehyde drops, and when the concentration is around 500 mg/L, the distillate can be considered as the heart part. The skill of the distiller consists of the ability to establish sensorially, and by habits regarding the alcohol flow, the moment the head of the distillate ends and, thus, they can begin to collect the so-called heart, which is the best part of the spirit, rich in ethyl alcohol and aromatic substances.

Historically, spirits producers measure the alcohol content of their products to ensure distillation monitoring. For this purpose, measuring the density followed by conversion into alcohol concentration using official alcohol tables is an officially recognized method for alcohol determination in distillates. Currently, the evaluation of the concentration of alcohol in beverages uses different recent techniques, such as an online digital density meter or infrared spectroscopy.[6] However, these types of equipment remain expensive. Some authors have focused on the development of ethanol soft sensors based on four temperature measurements and data processing, which are not yet commercially available for spirit beverage producers.[7] Moreover, the determination of more complex compounds such as acetaldehyde requires laboratory equipment, the most common being gas chromatography (GC) which, like UV−vis−IR spectroscopy or high-performance liquid chromatography (HPLC),[8,9] is an accurate methods. Unfortunately, this equipment is only found in a laboratory environment and is not available for online or in-line measurement.

In this context, EIS is an excellent option compared to traditional analysis methods since it allows real-time, in the field measurements, and is portable and easy to use.[10] So far, EIS has been proven as an interesting tool in the area of medicine but also in the field of food quality assessment, being used to characterize vegetables, fruits, and meat tissues in cell cultures as well as fermentation processes, to measure the biomass concentration, or to correlate physicochemical properties of thermally treated foods.[2] In the wine industry, for example, the EIS has been used to characterize different wine varieties, comparing the results with the standard chemical analysis. The results presented by Lopes et al.[3] show that the technique has a high potential in the wine industry, both to replace as well as to complement the traditional methods. Also, as shown by Leo et al.,[1] miniaturized EIS sensors with interdigitated (ID) electrodes, without any functionalization for ethanol sensing in liquid solutions, seem to be a viable alternative for investigating alcohol concentrations. On the same topic, Zheng et al.[11] have used EIS for studying the dielectric properties of ethanol and organic acids and found strong correlations between the concentrations of the pure solutions and their respective dielectric parameters. Often, only the capacitance values at a fixed frequency are considered to sense the amount of ethanol in a solution, which leaves space for more complex impedance analysis. As shown by Riul et al.,[12] the EIS data sometimes need to be processed by rather complex means, such as principal component analysis along with artificial neural networks, to interpret the results.

Nevertheless, some authors have noted that this technique has flaws in data processing and interpretation,[2] so it is necessary to automate its processing.[13] Also, several factors intrinsic to the solution under investigation can affect the obtained impedance spectra, as the liquid is still active and can interact with the coating of the measuring electrodes,[14] which is why the electrode materials along with the measurement procedures should be standardized for each particular measurement.

In this context, the objective of this work is to develop a new sensor for EIS measurement of wine-based distillation fractions. Along with data modeling (PLS-R), this sensor should be adapted for ethanol and acetaldehyde control during the production of spirit beverages.

EXPERIMENTAL METHODS

Sensor Manufacturing. The four sensors developed in this study were designed using Mentor Graphics and manufactured in PCB form by Cirly, France. Each sensor contains only one signal layer. All electrodes were manufactured using gold-plated copper (or copper alloys) in order to avoid the electrode oxidative degradation. Commercially available pins (M12 Crimp contact pin 0.8 mm, part 2314097 from TE Connectivity and pin contact size 12, part 1650060 from Tyco Electronics) were used for the "Header" sensors. The connection toward the measuring equipment was realized using coaxial cables and intermediary circular connector DIN 45326 to the BNC connector of the commercial impedance analyzer. The performance of these four sensors was first checked with a 20/80% (v/v) ethanol−water solution with an impedance analyzer and by FEM modeling.

Distillations of Wines. Nine commercial wines produced from different grape varieties (Chasselas, Sauvignon blanc, Chardonnay, Riesling, Cabernet sauvignon, Merlot) were used for the distillation. Distillations were conducted on a 25 L distillation pilot (Holstein, Germany) equipped with a mass flow meter, allowing precise process monitoring. Eighteen fractions of each distillation were collected successively. During measurement, the temperature of collected distillates was around 18 °C.

Reference Methods. GC-FID analysis of ethanol and acetaldehyde was used as reference method.[15]

Acetaldehyde (CAS 64-17-5) was provided by Merck KGaA (Darmstadt, Germany). HPLC grade ethanol was also purchased from Merck (Merck KGaA, Darmstadt, Germany). Deionized water (>18 MΩ) was obtained with a Millipore Treatment system (Millipore, Bedford, MA, USA). GC

https://doi.org/10.1021/acsomega.3c00481
ACS Omega 2023, 8, 15323−15333

separations were performed on a gas chromatograph Agilent 7890B (Agilent Technologies, Santa Clara, CA, USA) equipped with an autosampler 7693 (Agilent Technologies, Santa Clara, CA, USA). Ultrapure hydrogen was obtained from HG PRO LN (LNI Swissgas, Geneva, Switzerland). The capillary column was an Rt-WAX of 60 m × 0.53 mm, with a film thickness of 1.0 μm (Restek, Bellefonte, USA). The temperature of the injector was 100 °C. The oven was programmed for 35 °C for 5 min, increased by 1 °C/min to 65 °C, and then increased by 20 °C/min to 240 °C, followed by 5 min at the final temperature, for a total runtime of 48.75 min. The temperature of FID was 250 °C. The split ratio was 10:1, and the injection volume was 1 μL. The volatile compound was determined by direct injection.

Impedance Measurement. A Hioki IM3570 impedance analyzer (Hioki, Japan), with an accuracy of 0.1% for magnitude and 0.1 for phase measurements, was used in this work, along with several electrodes developed internally. A PC was used to control the impedance analyzer and interface as well as to collect the measured impedance spectra via an IEEE-488 GPIB cable (National Instruments, USA). The excitation voltage was set to 50 mV. A frequency sweep was performed between 20 Hz and 1 MHz, with a total of 400 selected frequencies, logarithmically spaced. The control software was developed using Python.

For each sample, 3 consecutive frequency sweeps were performed, and each spectrum was saved separately. An amount of 4 mL of testing sample, poured in a 5 mL hermetically sealed glass vial (Glaswarenfabrik Karl Hecht GmbH, Sondheim vor der Rhön, Germany), was used for each measurement. All the electrodes integrated to the 3d SLA printed lid (Figure 1) were completely immersed in the test

Figure 1. EIS measurement setup.

solution and placed at a 5 mm distance from the bottom of the glass container. According to the literature, dielectric properties of liquids, such as fruit juices, are temperature dependent.[16] Thus, all the samples were kept at a constant 18 °C during the signal acquisition, which was the temperature of the output of the distillates. The measurement of each solution sample took about 1 min, and the electrodes were wiped with an ethanol-soaked tissue and dried under open air before recording the impedance response of another sample.

For this work, 9 commercial wines were used for distillation, and 18 fractions of each distillation were collected. Thus, the impedance measurement of 162 samples in total was performed with the four developed sensors.

PLS-R Modeling. Three impedance-related parametres were measured and used to predict ethanol and acetaldehyde concentrations via PLS-R modeling: impedance (Z), phase (Φ), and capacitive contribution (Cp). In order to keep only one of the three repetitions of the impedance measurement, the Partial Curve Mapping (PCM) algorithm[17] was applied to remove the measurement most different from the others. As the next step, the measurement showing less noise, of the two remaining measurements, was used for modeling. Afterward, the Kennard−Stone algorithm was used on the 162 data sets to create "training" sets (90%; N = 146) and "validation" test sets (10%; N = 16). For the following step, the partial least-squares regression (PLS-R) algorithm was used to predict the compound value based on impedance measurement data, using the validation test sets. A custom software, created using Python programming language, was used for the calculations, using the "scikit-learn" machine learning library. The PLS-R model was set on the training data set and validated on the test data set, using the measured chemical values. The number of components of the principal component analysis (PCA) of the PLS-R was found by taking the one with less mean squared error (MSE) of the residual of a cross validation with the "leave-one-out" method on the training data sets.

To improve the PLS-R models, several preprocessing treatments were tested: standardization by removing the median and scales of the data according to the quantile range (RobustScaler), standard normal variate (STD) transformation, multiplicative scatter correction (MSC), and smoothing by the Savitzky−Golay filter (SG). The parameters of the filter were optimized by screening all the combinations of the length of the filter window from 2 to 40, the order of the polynomial, and the order of the derivative, from 0 to 5. To identify outliers in the training data, the data sets with the Z-score of the residual of the PLS-R with a "leave-one-out" cross-validation greater than 3 were removed. Also, to remove the impedance frequency regions with less interest for the PLS-R model, the coefficients of variable importance in the projection (VIP) based on the PLS-R model of the training data set were used. Furthermore, the regions with VIP metrics lower than one were removed. The order of the three data set transformations described above was permuted to find the most performant PLS-R model. Finally, by considering the preprocessing methods, outliers' identification methods, the impedance frequency region, and the process order, PLS-R models were trained with the training data set for each probe, for two EIS measurement parameters, all for each compound of interest (ethanol and acetaldehyde). The coefficient of determination (R^2), the root mean squared error of prediction (RMSEP), the bias (systematic error), and standard deviation (STD) were calculated on the residual of each predicted value of the test data set.

Simulation of Signal Transfer. The software Comsol Multiphysics (Comsol Inc., Sweden) was used for FEM modeling. The investigated liquid was set to be complex media, corresponding to the mix of a solution containing water, ethanol (70% v/v), and acetaldehyde (500 mg/L). The permittivity of the liquid mixture was calculated proportional and linear to the concentrations and dielectric permittivities of its constituents ($\varepsilon_{r\_complex}$ = 30.8). The average electric field in the liquid, along with the electric potential distributions, were computed for two distinct frequencies: 1.3 kHz and 1 MHz.

https://doi.org/10.1021/acsomega.3c00481
ACS Omega 2023, 8, 15323−15333

Except for the investigated complex liquid, for all the other materials, such as the PCB, copper, etc., the material constants (electrical conductivity, dielectric constant, etc.) were taken from the database of the software.

RESULTS AND DISCUSSION

Parameters and Conditions of EIS Measurement. In practical terms, EIS involves exciting a sample with frequency-variable electric sinusoidal signals and registering the system's response. The voltage $V(t)$ and current $I(t)$ across the specimen, at steady state, are sinusoidal functions of time and can be defined as periodic functions for a specific frequency ω, as follows:

$$\underline{V} = \hat{V}\cdot e^{j(\omega t+\Phi_V)} \tag{1}$$

$$\underline{I} = \hat{I}\cdot e^{j(\omega t+\Phi_I)} \tag{2}$$

where $\ddot{V}$ and $\ddot{I}$ are the peak voltage and, the peak current values, respectively, and Φ_V and Φ_I their phase shift with respect to $t = 0$. Also, $j = \sqrt{-1}$. By using Ohm's law, the following equation can be derived to define the impedance Z for a single frequency:

$$Z_\omega = \frac{\underline{V}}{\underline{I}} = \frac{\hat{V}}{\hat{I}}\cdot e^{j(\Phi_V-\Phi_I)} = |Z|\cdot e^{j\Phi} \tag{3}$$

where $|Z|$ is the impedance module in ohms (Ω) and Φ is the phase shift in radians. Since the impedance can be defined for any frequency, we get:

$$Z(\omega) = \frac{V(\omega)}{I(\omega)} \tag{4}$$

Furthermore, using Euler's relationship, impedance can also be defined as

$$Z(\omega) = Z'(\omega) + j\cdot Z'(\omega) = R(\omega) + j\cdot X(\omega) \tag{5}$$

where R is called the resistance, the real part, and X the reactance, the imaginary part. Thus, the impedance can be characterized as the opposition that materials manifest to the passage of an alternating electric current.

Based on the previous formulas, additional parameters such as the capacitive contribution (Cp) can be derived as

$$\mathrm{Cp} = \frac{-\sin(\Phi)}{\omega\cdot|Z^*|} \tag{6}$$

Because the impedance can vary with frequency, it can be seen as a three-dimensional quantity. As shown in Figure 2, plotting in two dimensions either requires two distinct plots (Bode plot) or making one of the dimensions implicit (the frequency, in a Nyquist plot).

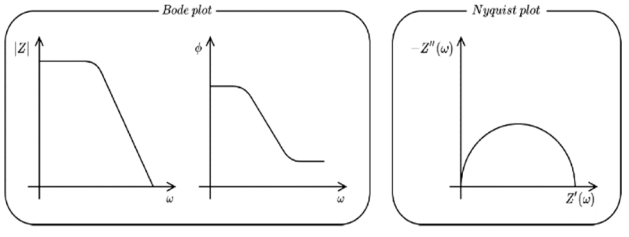

Figure 2. Two most common ways of representing impedance: Bode and Nyquist plots.

The reader should note that the convention used in EIS literature for the Y-axis of the Nyquist plot is the opposite of the one used in electrical engineering. This is because real-life biochemical systems will almost always exhibit a combination of resistive and capacitive behavior (although more complex elements, such as constant phase elements or Warburg impedances, can also be added), putting the data in the first quadrant when using the reversed Y-axis. Also, Nyquist plot representation is preferred for fitting impedance data to an electrical equivalent circuit (EQC) since it gives quick visual feedback in a single graph.

Measuring the impedance of a sample under test implies applying an AC voltage of constant amplitude over two points and measuring the current intensity through electrodes. Such a setup is called a "potentiostat" because the potential is controlled and the current through the sample varies according to its impedance. Reciprocally, the device keeping current at a constant amplitude while voltage varies freely is called a "galvanostat". In most cases, the investigation by potentiostat EIS or galvanostat EIS is equivalent and provides the same results, but, there are application-specific conditions, making one technique more suitable than the other. For example, in the case of corrosion analysis with the open-circuit voltage changing with time, galvanostat EIS assures the measurement is carried out at the true corrosion potential.[18]

Another important aspect is that the amplitude of the excitation signal must be chosen carefully. In theory, the amplitude should be kept as small as possible to stay in a pseudolinear region that prevents any nonlinear effects associated with the heating of the sample due to Joule losses. Excitation signal amplitude estimates indicate a 1 to less than 20 mV amplitude range[19] in order to stay within the pseudolinear region, although some publications mention the use of a 100 mV excitation signal, without specifying whether the linearity criterion was violated. In practice, using signals of such small amplitudes goes with a large deterioration of the signal-to-noise ratio (SNR), which is why the appropriate combination between excitation and SNR should be found for each specific application. At the same time, the nonlinear effect can be used to study the SUT by observing the amplitude and ranks of the generated harmonics, which might be unique to the nature of the sample. This relatively recent technique is referred to as nonlinear electrochemical impedance spectroscopy (NLEIS).[19,20] Last but not least, another issue related to the amplitude is the fact that the order of magnitude of the impedance to be measured might not be known beforehand. This means that the current might be several orders of magnitude lower for high-impedance samples compared to a lower impedance one. As a result, choosing an amplitude that yields good results for a given sample (as far as SNR goes) might not be appropriate for other samples, which is why the characteristics of the measurement should always be application based. After investigation, a 50 mV excitation voltage was validated and used in this work. Last but not least, the frequency sweep range is also important. In the case of complex materials, different components might exhibit different mobilities, and $Z(j\omega)$ is generally measured over a wide range of frequencies. The compositional complexity is the characteristic of distillation samples. Thus, a large frequency sweep, between 20 Hz and 1 MHz, was chosen in this study, with a total of 400 selected frequencies, logarithmically spaced.

Design of Sensors. EIS measurements can be made with a different number of electrodes in different configurations,

https://doi.org/10.1021/acsomega.3c00481
ACS Omega 2023, 8, 15323−15333

among which the most common ones are usually called two-, three-, and four-electrode implementations. Nevertheless, there are limitations to the basic two-electrode system, as the excitation signal is applied, and also the measurement is done using the same two electrodes. The limitation is mainly the fact that the impedance of the electrodes and their interface with the sample are included in the measurement. Switching to a four-electrode configuration removes most of the influence of the electrodes, thus making the measured impedance independent of the electrode−sample interfaces, as shown in Figure 3. In practice, the use of a higher number of electrodes

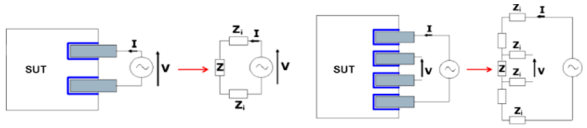

Figure 3. Circuit models for two- (left) and four-electrode (right) configurations, where Z_i represents the interface impedance.

makes the measurements more complex but also more precise. Thus, a trade-off is needed, the optimum solution depending on the constraints of the specific application.[18] A four-electrode configuration is used by all the sensors that we developed in this work.

In a recent study,[1] the electrical impedance spectroscopy (EIS) device employed for ethanol concentration evaluation was composed of a "2D" sensing module with interdigitated electrodes and an array of resin 3D printed chambers, which separated each sensing area. As shown by Leo et al.,[1] this structure is not unique, as a similar layout was previously used for biosensors and environmental sensor applications.[21−24] In another study,[25] focused on milk analysis, two stainless steel rods have been used to create a "3D" sensing structure, spaced 10 mm from each other and submerged to a depth of 20 mm. Smaller "3D" electrodes, needle like, have been proposed by other research teams.[26,27] Similar structures have also been presented in the literature, along with variations for electrode materials, such as gold or platinum, with or without thin polymer coatings, to improve the capacitive sensing capabilities of the sensor and reduce the magnitude of faradaic current flowing through the sensor.[2]

Based on the impact of number of electrodes and inspired by the various sensor and electrode designs found in the literature, our research group has designed four new EIS sensors (represented in Figure 4), with different sizes and shapes. All the EIS sensors present four-electrode configurations: two excitation (drive) electrodes and two sensing electrodes. Except for the sensing areas, all the energized parts that were exposed were covered by a silicon resin in order to electrically isolate them and also in order to limit the cross-talk between the electrodes as much as possible. Additionally, the "open" and "short" calibrations performed before the impedance measurements for each EIS sensor along with its connectors allowed us to further quantify and remove the parasitic RLC components that could influence the tests.

The first two electrodes, symmetrical and asymmetrical "Spots" (Figure 4a and b), represent a 2D design inspired by several studies.[18,2829] In this "four-electrode, four-pole design", with or without 2 different electrode surfaces (asymmetrical), the separation of voltage-inducing and current-measuring electrodes almost completely eliminates polarization issues and the influence of the cable resistance. However, the

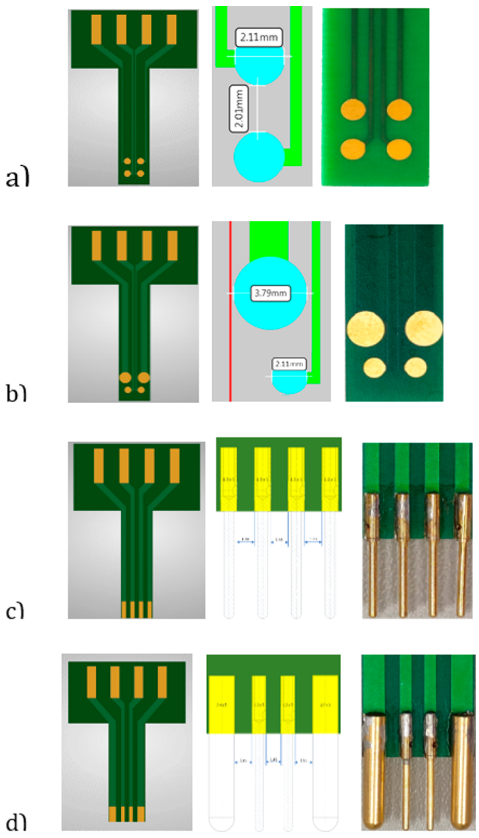

Figure 4. Four new EIS sensor designs presented in Gerber, CAD, and real sensors. Photos: (a) "SpotsSym", (b) "SpotsAsym", (c) "HeaderSym", and (d) "HeaderAsym".

capacitive influence remains and has to be compensated during calibration. By choosing electrodes that are asymmetrical, an inhomogeneity of the electric field at the voltage electrodes is expected. This allows for the cell constant of a four-pole system to be strongly influenced by the conductivity of the solution, as the transmitters working with a four-pole cell offer the input of different cell constants to cover the whole conductivity range.[29] In the "six-electrode, four-pole design" presented in the same references, drive and sensing electrodes have the same surface, allowing for a symmetrical configuration. While the corresponding electrical circuit is identical with the four-electrode, four-pole design, the big difference lies in the strength and homogeneity of the electrical field that is present around the voltage measuring electrodes. The more homogeneous field distribution in the area of the voltage electrodes results in a much less variable cell constant since the influence of the fringe effect is drastically reduced. The symmetrical design allows for a much higher field density and less sensitivity to field distortion.[29] Nevertheless, Tura et al.[30] also emphasize the advantages of using an asymmetrical electrode configuration, with larger drive electrodes, in order to increase the SNR, which is why it was decided to try a second electrode design with higher electrode surface, also in a symmetric and asymmetric configuration. Inspired by the needle-shaped electrodes found in the literature, a "3D linear" configuration (needle-shaped electrodes, placed in a row) was also proposed in this work, with the goal of further reducing the electrode polarization, compared to the "Spots".[29] The obtained sensors were named symmetrical and asymmetrical "Header" (Figure 4c and d) and were manufactured by soldering 4 pins over the

https://doi.org/10.1021/acsomega.3c00481
ACS Omega 2023, 8, 15323−15333

specifically designed conductive terminations found in the lower part of their corresponding PCBs.

The performance of the four sensors was first checked with a 20/80% (v/v) ethanol−water solution, using the impedance analyzer. The obtained Nyquist plots are depicted in Figure 5.

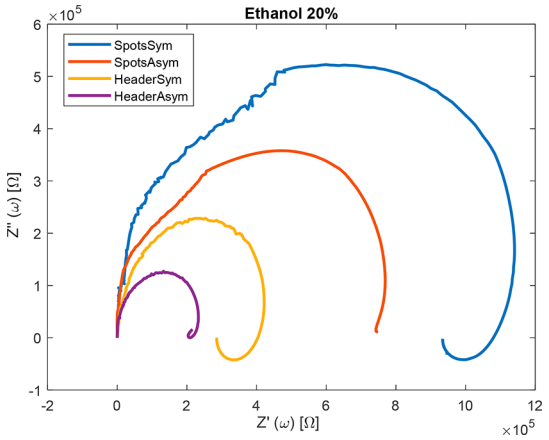

Figure 5. Nyquist plots for 20% v/v ethanol solution, measured with the four sensors designed in this work.

For this solution, the surface of the Nyquist half-circle plots is clearly dependent on the type of electrodes used for the sensor. A decrease in the measured impedance of the solution at high frequencies—and, also, in the corresponding surface of the Nyquist half-circle—is found for the "HeaderAsym" electrode. This result was to be expected since, as it will be further shown in the "Simulation of signal transfer" section, at 1 MHz, the "HeaderAsym" sensor showed the highest electric field, followed by "SpotsAsym", "HeaderSym", and "SpotsSym". This corresponds exactly to the size of the Nyquist half-circles.

Modeling Using PLS-R: Results Obtained for Wine-Based Distillates. Inspired by PLS-R calibration models based on near-infrared spectroscopy developed for the beverage industry, it was considered that this modeling approach could be adapted for impedance measurement data for component concentration prediction in a complex matrix. Thus, establishing acetaldehyde and ethanol concentration prediction models based on impedance measurement data was attempted, more specifically using these three parameters: impedance (Z), phase (Φ), and capacitive contribution (Cp).

Figure 6 illustrates the distribution of acetaldehyde and ethanol concentrations in 162 distillate samples, obtained with the reference method. Each curve represents the evolution of either component concentration in 18 successive collected fractions. The sample had ethanol concentrations ranging from 28.7% to 88.0% and acetaldehyde concentrations ranging from 0.0 mg/L to 2103.2 mg/L. For one of the orange curves, the concentration of acetaldehyde in the first fraction is much lower than the second fraction, which is uncommon. We assumed that this was due to human error when collecting the sample for measurement. However, this error does not impact the modeling work since the concentrations obtained with reference methods are correct. Some spikes observed in the decreasing tendency for ethanol and acetaldehyde concentration are due to the distillation dynamics, influenced by the base wine and Holstein pilot.

Table 1 summarizes the correlation coefficients obtained from PLS-R modeling without any data pretreatment. It is

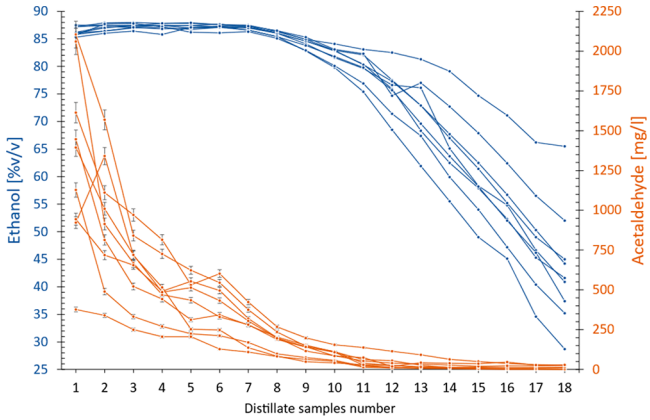

Figure 6. Distribution of acetaldehyde (orange curves) and ethanol (blue curves) concentrations in distillate samples, measured with reference methods.

shown that for acetaldehyde prediction the capacitance (Cp) parameter presented the best performance with positive R^2 values for all the tested sensors. For ethanol prediction, the combination of the phase shift (Φ) parameter for the "SpotsSym" sensor showed the highest R^2 value up to 86.84%. The sensor "SpotsAsym" showed mediocre performance for both component predictions, and both "Header" configuration sensors showed low potential for their capacity of ethanol concentration prediction. To sum up, the "SpotsSym" sensor configuration seemed to be the most performant for both acetaldehyde and ethanol concentration predictions, but with two different parameters (Cp and Φ). The two "Header" sensors also showed interesting potential for acetaldehyde concentration prediction with the Cp parameter.

Based on these results, in order to improve prediction performance, several data pretreatments were conducted, like preprocessing treatments, frequency filter, and outlier identification, as described in the Experimental Methods section.

Table 2 summarizes the results obtained for the improved models (R^2 > 80%) used for predicting acetaldehyde concentrations, including details on the pretreatments applied to the data and their order. With these pretreatments, the acetaldehyde concentration prediction performance of the "SpotsSym" sensor was widely ameliorated. The R^2 was increased from 69.90% to 89.94%. For this first model (R^2 = 89.94%), the impedance frequency was removed according to the VIP score (Figure 7). All frequency regions with a contribution score lower than 1 were eliminated. Four main frequency regions were kept (20 to 25 Hz, 700 Hz to 1.6 kHz, 31 kHz to 130 kHz, and 470 kHz to 1 MHz). Three outliers were eliminated by considering the "Z-score". The amelioration of prediction power of the two "Header" sensors was less significant after data pretreatments, from 84.54% to 85.81% for "HeaderSym" and from 81.39% to 83.66% for "HeaderAsym".

In order to further understand the correlations obtained in the first model for the "SpotsSym" electrode, the prediction versus the measured acetaldehyde values for testset data are plotted in Figure 8A. As shown, the acetaldehyde concentration prediction is rather accurate when the concentration is lower than 500 mg/L, whereas for higher concentrations the prediction should be improved. Nevertheless, the goal of monitoring acetaldehyde during spirits beverage production is to identify the point at which the acetaldehyde level drops to

https://doi.org/10.1021/acsomega.3c00481
ACS Omega 2023, 8, 15323−15333

Table 1. Correlation Coefficients (R^2) for Acetaldehyde and Ethanol Concentration Prediction Models According to Parameters, Without Any Impedance Data Pretreatment

Compound (prediction used parameter)	R^2 (SpotSym)	R^2 (SpotAsym)	R^2 (HeaderSym)	R^2 (HeaderAsym)
Acetaldehyde (Z)	−19.89%	−10.44%	−38.40%	−18.37%
Acetaldehyde (Φ)	38.45%	−13.08%	46.97%	68.18%
Acetaldehyde (Cp)	69.90%	27.82%	84.54%	81.39%
Ethanol (Z)	−3339.73%	3.68%	−2464.37%	−520.40%
Ethanol (Φ)	86.84%	−41.83%	3.12%	46.23%
Ethanol (Cp)	−231.47%	42.93%	−353.21%	−31.42%

Table 2. Acetaldehyde Concentration Prediction Models with R^2 > 80%

Sensor	Parameter	Treatment order	Preprocessing	Freq filter	Outlier (nb.)	RMSEP	R_2	Bias	SD
SpotsSym	Cp	OF	No	VIP	Z-score (3)	198.30	89.94%	−5.74	204.72
SpotsSym	Cp	O	No	No	Z-score (3)	208.41	88.88%	18.75	214.37
HeaderSym	Cp	OFP[a]	SG [40;3;0]	VIP	Z-score (3)	224.72	85.81%	32.28	229.68
HeaderSym	Cp	O	No	No	Z-score (3)	227.48	85.46%	29.26	232.99
HeaderSym	Cp		No	No	No	234.57	84.54%	27.67	240.57
HeaderAsym	Cp	FOP	SG [29;1;0]	VIP	Z-score (3)	264.41	83.66%	30.85	271.22
HeaderSym	Cp	F	SG [39;1;0]	No	No	244.91	83.15%	47.93	248.05
HeaderAsym	Cp	PFO	SG [40;1;0]	VIP	Z-score (4)	268.71	83.12%	−52.15	272.25
HeaderSym	Cp	POF	SG [39;1;0]	VIP	Z-score (3)	247.94	82.73%	4.80	256.03
HeaderAsym	Cp	F	No	VIP	No	272.30	82.67%	29.01	279.62
HeaderSym	Cp	PFO	SG [39;1;0]	VIP	Z-score (4)	255.16	81.71%	5.47	263.47
HeaderAsym	Cp	FPO	SG [25;1;0]	VIP	Z-score (3)	281.49	81.48%	29.24	289.15
HeaderAsym	Cp		No	No	No	282.14	81.39%	7.90	291.28

[a]OFP: the data treatment order is 1. Outlier elimination (O): 2. Filtration of impedance frequency (F): 3. Preprocessing treatment (P).

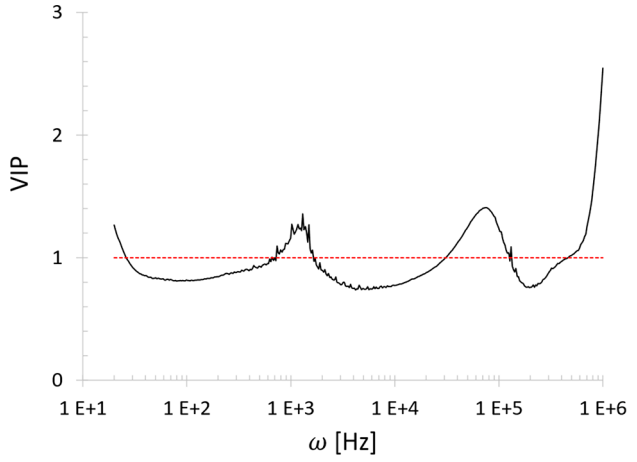

Figure 7. VIP score of different frequencies in PLS-R model for acetaldehyde concentration prediction with capacitance parameter measured with the "SpotsSym" sensor.

around 500 mg/L, which distinguishes the "head" and "heart" fractions of the distillate. Therefore, a precise concentration prediction outside this range is not necessary. As a result, our approach holds great potential for acetaldehyde monitoring during the distillation process. Furthermore, as shown by Figure 7, higher VIP scores are obtained in the high frequency regions in our study. Thus, expanding the higher frequency region should be considered for future development.

With respect to the ethanol concentration prediction, Table 3 synthesizes different models obtained after data pretreatments with R^2 > 75%. "SpotsSym" remained the only sensor with satisfactory performance in combination with the phase shift parameter (Φ). In this case, data pretreatments did not ameliorate the R^2 value, and the model obtained without any treatment remained the most performant. However, it should be noted that the model with the Savitzky−Golay filter showed lower bias than the model without any treatment.

Figure 8B displays the prediction results of the "SpotsSym" sensor for ethanol concentration. The prediction accuracy was found to be higher for higher ethanol concentrations, specifically in the range of 80% to 90%. During the distillation, the moment when the ethanol concentration drops to the range of 60%−70% indicates the end of the collection of the "heart" part and the beginning of the "tail" collection. Thus, additional samples with ethanol concentrations between 60% and 90% should be used in future studies to validate the ethanol monitoring model for distillation, with the potential for significantly improving prediction accuracy. Nevertheless, the current results are encouraging for further development.

Additionally, the capacitance and phase spectra for two series of 18 distillation fractions, measured using the "SpotsSym" sensor, are presented in Figure 9. The base wines for these two series of distillation are Riesling (series A) and Cabernet Sauvignon (series B). The spectra were distinguished by red to green gradual colors, according to the acetaldehyde (mg/L) and ethanol (% v/v) concentrations. In Figure 9A1, three distinct categories can be found by analyzing the capacitance spectra in the low frequency region, with respect to the decreasing acetaldehyde concentrations: 0−100 mg/L (green curves), 100−1000 mg/L (orange curves), and >1000 mg/L (red curves). However, this distinction is less clear in the second series (Figure 9B1), where the orange curves (100−1000 mg/L) and green curves (0−100 mg/L) overlap in the same frequency region. The same tendency can also be observed in the phase spectra (Figure 9A2 and Figure 9B2). These findings indicate that the matrix of base wines plays an important role in capacitance and phase spectra. Indeed, the molecular compositions of distillates of different

https://doi.org/10.1021/acsomega.3c00481
ACS Omega 2023, 8, 15323−15333

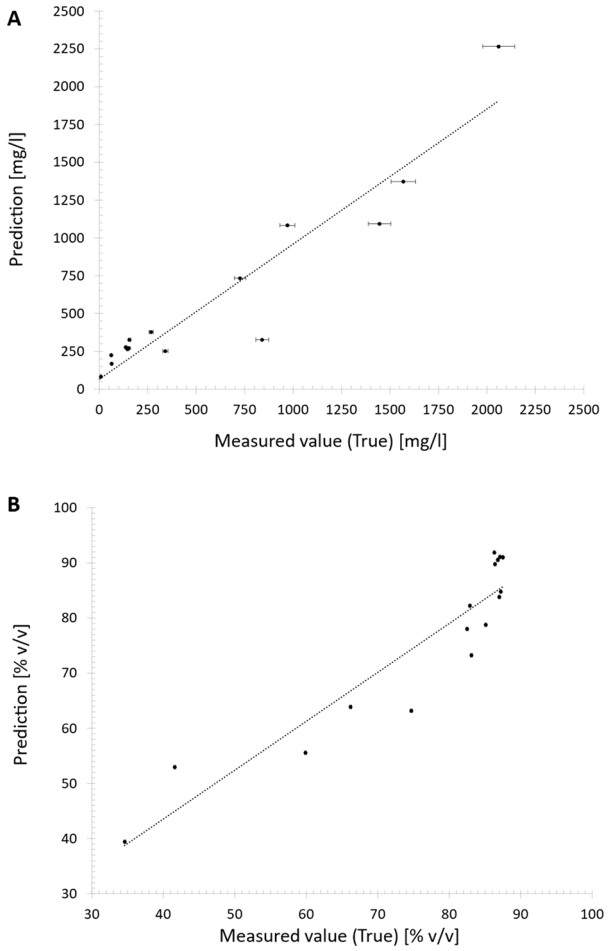

Figure 8. (A) Prediction versus measured values of the "SpotsSym" sensor for acetaldehyde (R^2 = 89.94%). (B) Prediction versus measured values of the "SpotsSym" sensor for ethanol (R^2 = 86.84%).

base wines are highly complex and diverse, consisting of various organic compounds such as alcohols, esters, aldehydes, ketones, acids, and phenolic compounds, among others. This complexity and diversity contribute to the unique aroma and flavor of each distillate. Therefore, to accurately predict acetaldehyde and ethanol concentrations in complex distillate matrices, multiple frequency regions should be considered by a modeling approach. In the case of acetaldehyde concentration prediction by PLS-R modeling, the exclusion of regions with lower VIP scores improved the performance. These frequency regions should be validated with a larger number of samples when it comes to another specific spirit application, for example, for kirsch or whisky production monitoring.

By combining the results obtained for both acetaldehyde and ethanol predictions, it can be concluded that the "SpotsSym" electrode configuration is the most adapted to our type of solution investigation. This points toward the use of a configuration allowing for a large electric field variation during the measurement, as the electric field decreases by a factor of two between the minimum and the maximum frequency range (see Table 4). This versatility allows for both smaller and larger molecules to respond to the excitation signal and thus obtain a better characterization of the investigated solution.

In summary, the PLS-R modeling of the EIS measurements obtained with the "SpotsSym" probe showed promising performance for acetaldehyde and ethanol concentration prediction. Also, the capacitance and the phase shift have been identified as the most suitable measurement parameters for this application. The next step of this study will be the development of a prototype for in-line acetaldehyde and ethanol monitoring.

Simulation of Signal Transfer. In order to further compare the four electrode designs and to have information regarding the performances of the various EIS sensors proposed in this work, Comsol software was used to compute the voltage and the electric field distributions obtained in the investigated solutions, for each sensor. Following the simulations, the average electric field in the liquid was calculated, for two distinct frequencies: 1.3 kHz and 1 MHz. These two frequencies were chosen according to the two highest asymptotes of the VIP score for acetaldehyde concentration prediction illustrated by Figure 7. As an example, the voltage distribution, in a configuration having 50 mV potential on the drive electrodes, with grounded sensing electrodes and floating potential considered for surrounding the complex ethanol, water, and acetaldehyde solution, is represented in Figure 10. The average electric field norms, calculated over the liquid volume, both at 1.3 kHz and 1 MHz, are given in Table 4. By analyzing the values given in Table 4, it can be found that for the "2D" electrode designs—the two "Spots" sensors—for which the fringing electric field is dominant a significant difference in terms of total average electric field could be found while comparing the lower and the higher frequency. As expected, for the "Spot" sensors, the electric field decreases when the frequency increases. Furthermore, the asymmetrical configuration allows for higher average electric fields in the investigated solutions, for both frequencies, pointing toward lower impedance values and

Table 3. Ethanol Concentration Prediction Models with R^2 > 75%

Sensor	Parameter	Treatment order	Preprocessing	Freq. filter	Outlier (nb.)	RMSEP	R^2	Bias	SD
SpotsSym	PHASE		No	No	No	5.95	86.84%	0.54	6.12
SpotsSym	PHASE	P	SG [34;2;1]	No	No	6.02	86.55%	0.28	6.21
SpotsSym	PHASE	O	No	No	Z-score (2)	6.46	84.52%	0.94	6.60
SpotsSym	PHASE	P	SNV	No	No	6.85	82.57%	0.99	7.00
SpotsSym	PHASE	OP	SNV	No	Z-score (2)	7.31	80.14%	1.59	7.37
SpotsSym	PHASE	F	No	VIP	No	7.60	78.55%	−0.25	7.85
SpotsSym	PHASE	PO	SNV	No	Z-score (2)	7.77	77.60%	1.21	7.92
SpotsSym	PHASE	POF	SNV	VIP	Z-score (2)	7.77	77.57%	1.55	7.87
SpotsSym	PHASE	PF	SNV	VIP	No	7.96	76.48%	1.20	8.13
SpotsSym	PHASE	FP	SNV	VIP	No	8.01	76.19%	2.06	7.99
SpotsSym	PHASE	FPO	SNV	VIP	Z-score (1)	8.09	75.72%	1.94	8.11

https://doi.org/10.1021/acsomega.3c00481
ACS Omega 2023, 8, 15323−15333

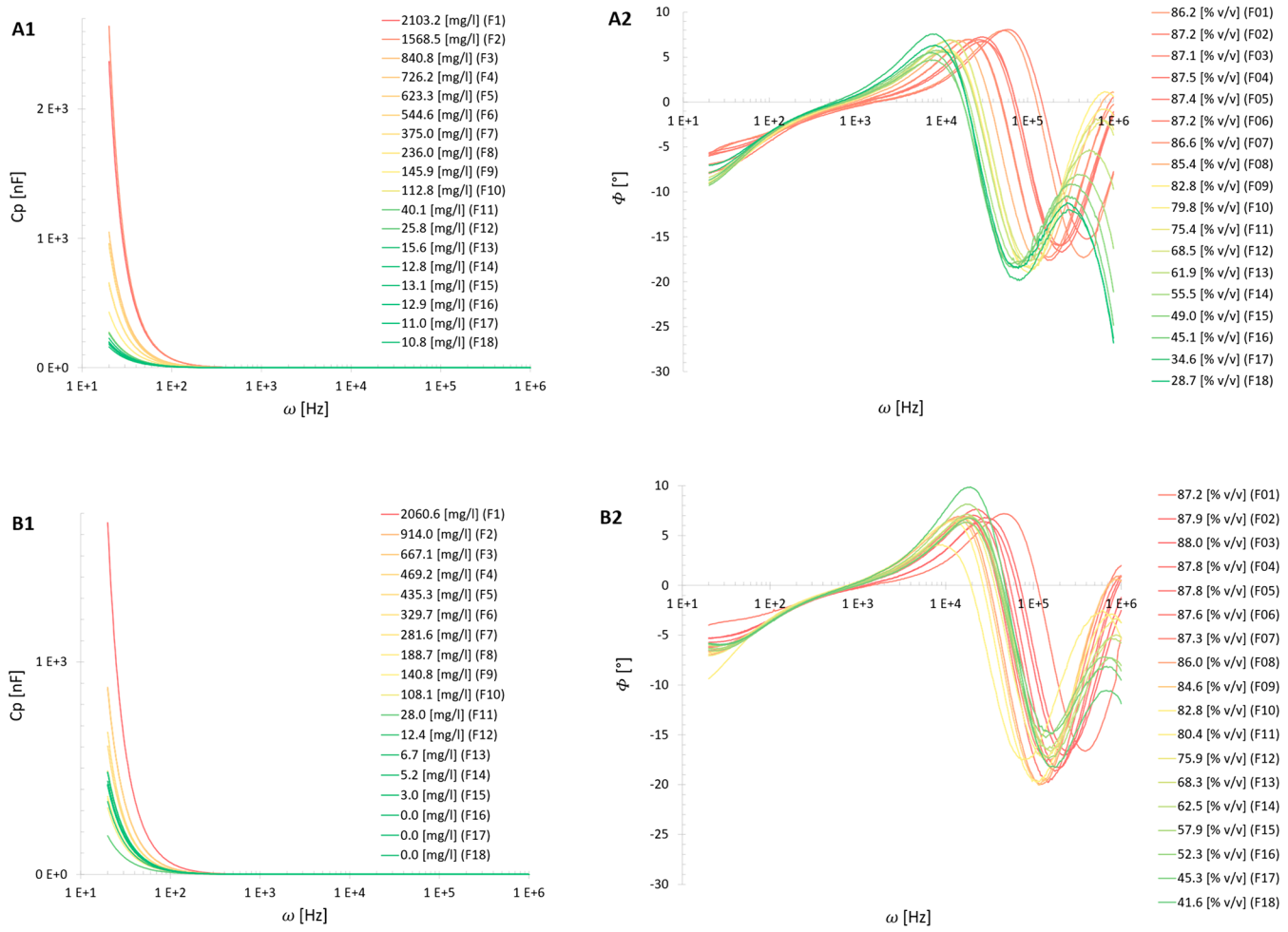

Figure 9. Capacitance spectra (left) and phase spectra (right) of two series of 18 distillation fractions measured with a "SpotsSym" sensor, distinguished by red to green gradual colors according to the acetaldehyde (mg/L) and ethanol (% v/v) concentrations. (A) Spectra of Riesling base wine distillation fractions. (B) Spectra of Cabernet Sauvignon base wine distillation fractions.

Table 4. Average Electric Field Norm Calculated over a Solution Containing Water, Ethanol (70% v/v), and Acetaldehyde (500 mg/L)

	Electric field norm (V/m)	
	1.3 kHz	1 MHz
SpotsSym	1.48	0.60
SpotsAsym	1.54	0.79
HeaderSym	0.61	0.65
HeaderAsym	1.21	1.27

higher sensitivity to noise, as previously discussed in the Design of Sensors section.

As shown in Table 4, in one extent the results obtained for the "3D" electrode designs—the two "Header" sensors—are different from those obtained for the "Spots". Although the asymmetric configuration allows for higher electric fields in both cases, for these configurations, the electric field increases slightly with the frequency due to the capacitive coupling effect, which is not the case for the "Spots". This is not a surprising result as in the "2D" configuration the fringing electric field is strongly influenced by the FR4 (the dielectric material which constitutes the PCB board) and its low permittivity (ε_r = 3.6), whereas in the "3D" configuration the field is influenced by the rather high permittivity of the solution (ε_r = 30.8).

The configurations with the highest voltage distributed over the sensor (symmetrical and asymmetrical "Spots", as shown in Figure 10) are also those exhibiting the highest average electric field over the whole volume of the solution. Based on these results, the "Spots" sensors seem to be the most interesting, with the "HeaderSym" the least interesting design, from an electrical field point of view.

CONCLUSIONS

This study investigated the potential of combining EIS measurements with PLS-R modeling to develop a low-cost monitoring system for spirit beverage production. Among the four sensor configurations, the "SpotSym", a "2D" sensor, with symmetrical disc-shaped electrodes, demonstrated the best results for determining acetaldehyde and ethanol concentrations, with correlations exceeding 86%.

Today, most EIS investigations are carried out using dedicated lab instruments (frequency response analyzers and LCR meters) as we also did in this study. However, they are expensive, must be used in a lab environment, and are not suitable for online measurements in the field.[18] Smaller, cheaper, and portable analyzers, based, for example, on Analog Device's AD5940, could be developed, which could represent

https://doi.org/10.1021/acsomega.3c00481
ACS Omega 2023, 8, 15323−15333

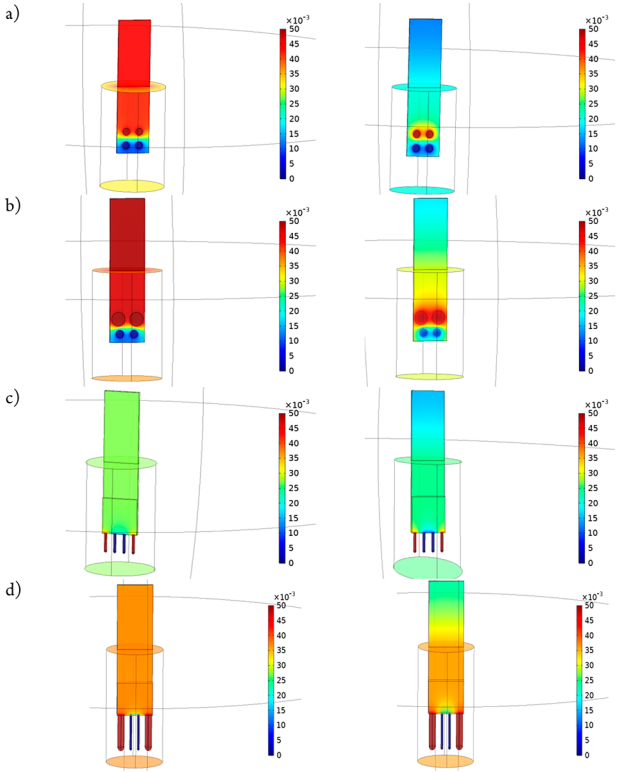

Figure 10. Electric potential distribution for the sensor and the top and bottom part of the surrounding complex liquid, at 1.3 kHz and 1 MHz for (a) "SpotsSym", (b) "SpotsAsym", (c) "HeaderSym", and (d) "HeaderAsym".

simple and cost-effective alternatives for developing new EIS in-line measuring setups.

However, it is important to note that the dielectric properties of liquids, such as fruits juices, are temperature-dependent.[16] Therefore, particular attention should be paid to validating the future in-line solution for the 10−18 °C temperature range commonly found in distillate outputs. Additionally, expanding to the higher-frequency region should be considered for future development, not only to improve accuracy of acetaldehyde measurement but also to include measurement of other critical components such as methanol.[31]

To our knowledge, this is the first report of sensors capable of simultaneously measuring ethanol and acetaldehyde concentrations. Furthermore, these sensors offer the advantages of being low cost and nondestructive, which is why a larger number of samples including different spirit beverages distillation fractions, like whisky, rum, kirsch, etc., can be used to create adapted PLS-R models.

AUTHOR INFORMATION

Corresponding Author

Liming Zeng − *Changins Viticulture and Enology College, University of Applied Sciences and Arts of Western Switzerland (HES-SO), Nyon, Switzerland;* orcid.org/0000-0002-9836-5491; Email: liming.zeng@changins.ch

Authors

Arnaud Pernet − *Changins Viticulture and Enology College, University of Applied Sciences and Arts of Western Switzerland (HES-SO), Nyon, Switzerland*

Marilyn Cléroux − *Changins Viticulture and Enology College, University of Applied Sciences and Arts of Western Switzerland (HES-SO), Nyon, Switzerland*

Benoît Bach − *Changins Viticulture and Enology College, University of Applied Sciences and Arts of Western Switzerland (HES-SO), Nyon, Switzerland*

Lucas Froidevaux − *iPrint Institute, University of Applied Sciences and Arts of Western Switzerland (HES-SO), Fribourg, Switzerland*

Ioana Preda − *iPrint Institute, University of Applied Sciences and Arts of Western Switzerland (HES-SO), Fribourg, Switzerland*

Complete contact information is available at: https://pubs.acs.org/10.1021/acsomega.3c00481

Author Contributions

The manuscript was written through contributions of all authors. All authors have given approval to the final version of the manuscript.

Funding

This project was funded by University of Applied Sciences and Arts of Western Switzerland (HES-SO), field of engineering and architecture through the project "WinE-index" (99633).

Notes

The authors declare no competing financial interest.

ACKNOWLEDGMENTS

The authors thank Nicolas Bapst for his initial contribution to the project.

ABBREVIATIONS

CPE	constant phase element
EIS	electrical impedance spectroscopy
EQC	equivalent circuit
FEM	finite element modeling
GC	gas chromatography
GC-FID	gas chromatography flame ionization detector
HPLC	high-performance liquid chromatography
IARC	International Agency for Research on Cancer
ID	interdigitated
IR	infrared
MSC	multiplicative scatter correction
MSE	mean squared error
NLEIS	nonlinear electrochemical impedance spectroscopy
PCA	principal component analysis
PCB	printed circuit board
PCM	partial curve mapping
PLS	partial least-squares
PLS-R	partial least-squares regression
RMSEP	root mean squared error of prediction
SLA	stereolithography
SNR	signal-to-noise ratio
SNV	standard normal variates
STD	standard derivation
SUT	Sample Under Test
UV	ultraviolet
VIP	variable importance in the projection
Vis	visible

REFERENCES

(1) Leo, A.; Monteduro, A. G.; Rizzato, S.; Milone, A.; Maruccio, G. Miniaturized sensors for detection of ethanol in water based on

electrical impedance spectroscopy and resonant perturbation method-A comparative study. *Sensors* **2022**, *22*, 2742.
(2) Caicedo-Eraso, J. C.; Díaz-Arango, F. O.; Osorio-Alturo, A. Electrical impedance spectroscopy applied to food industry quality control. *Ciencia y Tecnología Agropecuaria* **2020**, *21* (1), 100−119.
(3) Lopes, A. M.; Machado, J. A. T.; Ramalho, E. On the fractional-order modeling of wine. *Eur. Food Res. Technol.* **2017**, *243* (6), 921−929.
(4) Liu, S.-Q.; Pilone, G. J. An overview of formation and roles of acetaldehyde in winemaking with emphasis on microbiological implications. *Int. J. Food Sci. Technol.* **2000**, *35* (1), 49−61.
(5) IARC. IARC monographs on the identification of carcinogenic hazards to humans. List of Classifications. In *Agents classified by the IARC Monographs*; 1999; Vol. *1*−*130*.
(6) Abbas, O.; Pissard, A.; Baeten, V. 3 - Near-infrared, mid-infrared, and Raman spectroscopy. In *Chem. Anal. Food*; Pico, Y., Ed.; Academic Press, 2020; pp 77−134.
(7) Osorio, D.; Ricardo Pérez-Correa, J.; Agosin, E.; Cabrera, M. Soft-sensor for on-line estimation of ethanol concentrations in wine stills. *J. Food Eng.* **2008**, *87* (4), 571−577.
(8) Cavinato, A. G.; Mayes, D. M.; Ge, Z. H.; Callis, J. B. Noninvasive method for monitoring ethanol in fermentation processes using fiber-optic near-infrared spectroscopy. *Anal. Chem.* **1990**, *62* (18), 1977−1982.
(9) Michel, K.; Bureau, B.; Boussard-Plédel, C.; Jouan, T.; Adam, J. L.; Staubmann, K.; Baumann, T. Monitoring of pollutant in waste water by infrared spectroscopy using chalcogenide glass optical fibers. *Sens. Actuators B: Chem.* **2004**, *101* (1), 252−259.
(10) El Khaled, D.; Castellano, N. N.; Gazquez, J. A.; García Salvador, R. M.; Manzano-Agugliaro, F. Cleaner quality control system using bioimpedance methods: a review for fruits and vegetables. *J. Clean. Prod.* **2017**, *140*, 1749−1762.
(11) Zheng, S.; Fang, Q.; Cosic, I. An investigation on dielectric properties of major constituents of grape must using electrochemical impedance spectroscopy. *Eur. Food Res. Technol.* **2009**, *229* (6), 887−897.
(12) Riul, A.; de Sousa, H. C.; Malmegrim, R. R.; dos Santos, D. S.; Carvalho, A. C. P. L. F.; Fonseca, F. J.; Oliveira, O. N.; Mattoso, L. H. C. Wine classification by taste sensors made from ultra-thin films and using neural networks. *Sens. Actuators B: Chem.* **2004**, *98* (1), 77−82.
(13) Pliquett, U. Bioimpedance: a review for food processing. *Food Eng. Rev.* **2010**, *2* (2), 74−94.
(14) Jorge, J.; Pereira, J. C.; Rodríguez, M.; N, B.; Oliva, D.; Antonio, J. Impedance spectroscopy in water/oil emulsions in a range of intermediate frequencies. *Ingeniería UC* **2018**, *25* (3), 388−395.
(15) Charapitsa, S. V.; Kavalenka, A. N.; Kulevich, N. V.; Makoed, N. M.; Mazanik, A. L.; Sytova, S. N.; Zayats, N. I.; Kotov, Y. N. Direct Determination of Volatile Compounds in Spirit Drinks by Gas Chromatography. *J. Agric. Food Chem.* **2013**, *61* (12), 2950−2956.
(16) Zhu, X.; Guo, W.; Wu, X. Frequency- and temperature-dependent dielectric properties of fruit juices associated with pasteurization by dielectric heating. *J. Food Eng.* **2012**, *109* (2), 258−266.
(17) Witowski, K.; Stander, N. Parameter identification of hysteretic models using partial curve mapping. In *12th AIAA Aviation Technology, Integration, and Operations (ATIO) Conference and 14th AIAA/ISSMO Multidisciplinary Analysis and Optimization Conference*; Aviation Technology, Integration, and Operations (ATIO) Conferences, American Institute of Aeronautics and Astronautics, 2012.
(18) Grossi, M.; Riccò, B. Electrical impedance spectroscopy (EIS) for biological analysis and food characterization: a review. *J. Sens. Sens. Syst.* **2017**, *6* (2), 303−325.
(19) Fasmin, F.; Srinivasan, R. Review—Nonlinear electrochemical impedance spectroscopy. *J. Electrochem. Soc.* **2017**, *164* (7), H443.
(20) Wilson, J. R.; Schwartz, D. T.; Adler, S. B. Nonlinear electrochemical impedance spectroscopy for solid oxide fuel cell cathode materials. *Electrochim. Acta* **2006**, *51* (8), 1389−1402.
(21) Piccinno, E.; Monteduro, A. G.; Dituri, F.; Rizzato, S.; Giannelli, G.; Maruccio, G. Validation of a Lab-on-Chip Assay for Measuring Sorafenib Effectiveness on HCC Cell Proliferation. *Int. J. Mol. Sci.* **2021**, *22* (23), 13090.
(22) Chiriacò, M. S.; Rizzato, S.; Primiceri, E.; Spagnolo, S.; Monteduro, A. G.; Ferrara, F.; Maruccio, G. Optimization of SAW and EIS sensors suitable for environmental particulate monitoring. *Microelectron. Eng.* **2018**, *202*, 31−36.
(23) Chiriacò, M. S.; Primiceri, E.; De Feo, F.; Montanaro, A.; Monteduro, A. G.; Tinelli, A.; Megha, M.; Carati, D.; Maruccio, G. Simultaneous detection of multiple lower genital tract pathogens by an impedimetric immunochip. *Biosens. Bioelectron.* **2016**, *79*, 9−14.
(24) Chiriacò, M. S.; Primiceri, E.; Monteduro, A. G.; Bove, A.; Leporatti, S.; Capello, M.; Ferri-Borgogno, S.; Rinaldi, R.; Novelli, F.; Maruccio, G. Towards pancreatic cancer diagnosis using EIS biochips. *Lab Chip* **2013**, *13* (4), 730−734.
(25) Durante, G.; Becari, W.; Lima, F. A. S.; Peres, H. E. M. Electrical impedance sensor for real-Time retection of bovine milk adulteration. *IEEE Sensors Journal* **2016**, *16* (4), 861−865.
(26) Watanabe, T.; Ando, Y.; Orikasa, T.; Shiina, T.; Kohyama, K. Effect of short time heating on the mechanical fracture and electrical impedance properties of spinach (Spinacia oleracea L.). *J. Food Eng.* **2017**, *194*, 9−14.
(27) Fernández-Segovia, I.; Fuentes, A.; Aliño, M.; Masot, R.; Alcañiz, M.; Barat, J. M. Detection of frozen-thawed salmon (Salmo salar) by a rapid low-cost method. *J. Food Eng.* **2012**, *113* (2), 210−216.
(28) Chiang, S.; Eschbach, M.; Knapp, R.; Holden, B.; Miesse, A.; Schwaitzberg, S.; Titus, A. Electrical impedance characterization of in vivo porcine tissue using machine learning. *J. Electr. Bioimpedance* **2021**, *12* (1), 26−33.
(29) *Conductivity: Electrodes, Poles and their effects on Conductivity.* https://www.optek.com/en/electrodes-and-poles-effects-on-conductivity.asp (accessed 2022 16/04).
(30) Tura, A.; Sbrignadello, S.; Barison, S.; Conti, S.; Pacini, G. Impedance spectroscopy of solutions at physiological glucose concentrations. *Biophys. Chem.* **2007**, *129* (2−3), 235−241.
(31) Pineau, N. J.; Magro, L.; van den Broek, J.; Anderhub, P.; Güntner, A. T.; Pratsinis, S. E. Spirit Distillation: Monitoring Methanol Formation with a Hand-Held Device. *Food Sci. & Technol.* **2021**, *1* (5), 839−844.

https://doi.org/10.1021/acsomega.3c00481
ACS Omega 2023, 8, 15323−15333